

Generation of confinement and other nonperturbative effects by infrared gluonic degrees of freedom

Michael Engelhardt^a

^aPhysics Department, New Mexico State University,
Las Cruces, NM 88003, U.S.A.

Recent progress in understanding the emergence of confinement and other nonperturbative effects in the strong interaction vacuum is reviewed. Special emphasis is placed on the role of different types of collective infrared gluonic degrees of freedom in this respect. After a survey of complementary approaches, models of the QCD vacuum based on center vortices, Abelian magnetic monopoles and topological charge lumps such as instantons, merons and calorons are examined. Both the physical mechanisms governing these models as well as recent lattice studies of the respective degrees of freedom are reviewed.

1. INTRODUCTION

Strong interaction physics is characterized by a range of nonperturbative phenomena. Quarks and gluons are confined into color singlet hadrons. Chiral symmetry is realized in the Goldstone mode, which decisively influences low-energy hadronic physics through the associated (quasi-) Goldstone bosons, i.e., the pions. On the other hand, the axial $U_A(1)$ part of the flavor symmetry is broken by an anomaly which manifests itself e.g. in the large mass of the corresponding flavor singlet pseudoscalar η' meson. This review is concerned with recent progress in understanding the QCD vacuum structure which leads to the emergence of such phenomena. While the primary emphasis is on confinement, also the other nonperturbative effects highlighted above are taken into account; a cogent picture of the QCD vacuum should provide a comprehensive explanation of these phenomena on a unified footing, rather than a collection of separate mechanisms.

This review particularly focuses on lattice studies of the role of different types of collective infrared gluonic degrees of freedom in generating the above nonperturbative effects. A variety of such degrees of freedom have been considered, which can be roughly classified according to their dimensionality in four-dimensional space-time:

Center vortices: Two-dimensional world-surfaces of quantized chromomagnetic flux.

Abelian magnetic monopoles: One-dimensional world-lines of sources and sinks of chromomagnetic flux.

Instantons, Merons, Calorons: Localized (i.e., zero-dimensional) lumps of topological charge (for calorons, this classification is not as clear-cut as for instantons and merons, since calorons generically consist of several distributed constituents).

In keeping with the review character of this contribution, before proceeding with the discussion of the aforementioned collective infrared degrees of freedom, a survey of complementary recent lattice investigations of confinement is in order. The reader's attention is also drawn to the recent review article by Greensite [1], which the present contribution has significant overlap with, in particular as far as center vortices and Abelian monopoles are concerned; [1] does not discuss the topological charge lumps mentioned above, but on the other hand delves more deeply into some of the subjects which are only touched upon in the following survey.

2. SURVEY OF RELATED WORK

The following are the pertinent lines of investigation on which there has been hep-lat archive posting activity since the previous Lattice Symposium (the author has made every effort to make

this survey complete in that sense):

Confinement in the Coulomb gauge: Confining behavior of the gluon propagator in Coulomb gauge has been shown to be linked to a remnant gauge symmetry being realized; an order parameter associated with this symmetry was introduced and studied [2]. The color Coulomb potential induced by the Coulomb propagator, which is an upper bound for the static potential between color sources, is linear both in the confined and the high-temperature deconfined phase of SU(2) Yang-Mills theory [2]. The Coulomb propagator, the ghost form factor and the color Coulomb potential have moreover been investigated in [3].

Confinement in the Landau gauge, Kugo-Ojima confinement criterion: Extensive studies of the gluon propagator, the ghost propagator and the associated running coupling have been performed in the Landau gauge [4,5,6,7]. One of these studies [4] in particular evaluated the Kugo-Ojima confinement parameter, obtaining the value -0.83 . Another investigation [5] focused on the effects of dynamical quarks, finding a reduction of the infrared enhancement of the gluon propagator. Evidence for violation of reflection positivity in the gluon propagator, interpreted as a manifestation of confinement, was reported in a large-volume three-dimensional study [6]. The Landau gauge properties in an ensemble generated by removing center projection vortices from the full SU(2) Yang-Mills ensemble were also considered [7]. In this case, the signatures of confinement in Landau gauge propagators disappear.

Confinement in models with exceptional gauge groups: The study of confinement in models with exceptional gauge groups is particularly interesting due to the fact that some gauge groups exclude certain confinement mechanisms because of their internal topology. The confining G(2) theory [8] has a trivial center and no center

vortices (G(2) is its own universal covering group and its first homotopy group is trivial, $\pi_1[G(2)] = \{0\}$). Moreover, by introducing an appropriate Higgs field, the G(2) gauge symmetry can be "broken" to SU(3) and the transition between exceptional and ordinary confinement can be studied. Also the Sp(2) and Sp(3) models have been considered [9]. In the case of Sp(2) in 2+1 dimensions, the Svetitsky-Yaffe conjecture is applicable and confirmed numerically.

SU(2) vs. SO(3) gauge groups: Comparing models with the SU(2) and the SO(3) gauge groups is instructive, since they obey the same algebra and only differ in their center (the SO(3) gauge group, despite its trivial center, nevertheless supports the equivalent of SU(2) center vortices; the universal covering group of SO(3) is SU(2), with the center $Z(2)$, and $\pi_1[SU(2)/Z(2)] = Z(2)$). The correspondence between the two models was elucidated in detail [10], where an analytic path connecting SO(3) and SU(2) lattice gauge theory at weak coupling was given. A recent study [11] focused on the deconfinement transition in a modified SO(3) model, finding a correspondence of critical exponents to the SU(2) theory; also Abelian magnetic monopole condensation was considered in [11], and found to be correlated with the presence of confinement.

Higher representation Wilson loops: An important characteristic of the Yang-Mills vacuum, useful to constrain vacuum models, is the behavior of higher representation Wilson loops. Direct evidence has been presented that the spectrum of string tensions in SU(3) Yang-Mills theory behaves according to n -ality [12]. Also higher numbers of colors have been investigated [13], finding k -string tensions lying between the MQCD and Casimir scaling conjectures.

Connecting short to long scales by decimations: A representation of the Yang-Mills partition function in terms of

successive decimations has been derived [14]. In this way, the short and long distance regimes of $SU(N)$ lattice gauge theory can be connected, with the aim of deriving exact statements about confinement.

String breaking: Breaking of the adjoint chromoelectric string at large distances has been observed in 2+1-dimensional $SU(2)$ Yang-Mills theory without resorting to a two-channel analysis [15], by exploiting a noise reduction method of the Luscher-Weisz type [16] to measure Wilson loops. Also fundamental string breaking in the presence of dynamical quarks at finite temperatures has been studied [17].

String-like behavior of the chromoelectric flux tube: Sparked by the introduction of the Luscher-Weisz noise reduction technique [16], which permits the evaluation of Wilson loops with unprecedented accuracy, this has been the most active of the lines of investigation surveyed here. A number of high precision studies of the static quark-antiquark potential have been undertaken [18,19,20,21,22,23,24] in both 2+1 and 3+1 dimensions, using $SU(2)$, $SU(3)$, $Z(2)$ and compact $U(1)$ gauge groups. The aim of these studies lies in extracting subleading contributions to the potential, such as the Luscher term, in order to search for string-like behavior of the chromoelectric flux tube. Bosonic string characteristics are found. In addition, the analogue of the Luscher term in the baryonic case has been computed [25] in 2+1 dimensions.

3. COLLECTIVE INFRARED GLUONIC DEGREES OF FREEDOM

The following questions are a useful guide in considering the relevance of the different types of infrared gluonic degrees of freedom which have been studied:

Can the degrees of freedom in question generate the nonperturbative ef-

fects characterizing the strong interaction in the infrared? How? If a particular set of degrees of freedom is to faithfully represent the infrared structure of the QCD vacuum, it should ideally supply a comprehensive account of the effects induced by that vacuum, rather than explaining only particular aspects.

Is it realistic to assume them to be weakly coupled/correlated? Infrared QCD vacuum structure can in principle be expanded in any suitably complete set of degrees of freedom; a relevant set should satisfy a more stringent criterion, namely that it generate the nonperturbative phenomena characterizing the strong interaction on the basis of a weakly coupled dynamics. Strong correlations between degrees of freedom in a given set are a signature that they are really combined into a different set of collective degrees of freedom which more faithfully represent the QCD vacuum.

How can they be studied in lattice gauge theory and what are the results of such studies? To further constrain the description of vacuum structure, it is useful to find ways of identifying different sets of infrared gluonic degrees of freedom in lattice gauge configurations and thus be able to investigate their structure and relevance directly in the full theory, complementing model studies which have to rely on their phenomenological results to justify the use of a particular set of degrees of freedom.

3.1. Center vortices

In four-dimensional space-time, center vortices are represented by closed two-dimensional world-surfaces (with a transverse thickness related to the QCD scale). Their flux is quantized; for $SU(N)$ color, there are $N-1$ types of flux, characterized by yielding one of the $N-1$ different nontrivial center elements of $SU(N)$ when a Wilson loop encircling the vortex flux is evaluated. The center vortex picture of the strong interaction vacuum assumes the vortex world-surfaces

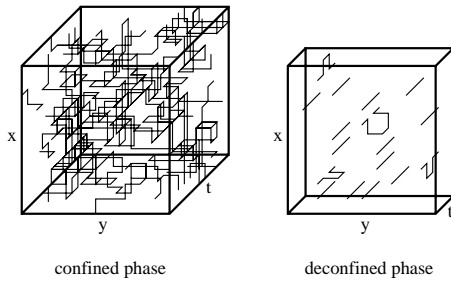


Figure 1. Typical vortex configurations in the confined and deconfined phases; one spatial coordinate is kept fixed.

to be weakly correlated, random surfaces on infrared length scales.

3.1.1. Confinement

On this basis, both the confined and the deconfined phases can be understood; a particularly intuitive picture is obtained by considering a slice of the universe in which one of the spatial coordinates is kept constant, cf. Fig. 1. At finite temperatures, when the time direction of (Euclidean) space-time becomes too short, the vortices cannot fluctuate appreciably in the spatial directions before closing on themselves by virtue of the periodic boundary conditions. They extend chiefly in the time and one space direction and cease to percolate (in the sliced universe depicted in Fig. 1). As will be seen presently, percolation is a prerequisite for confinement. The deconfining transition can be understood as a percolation transition induced by the change in entropy of the random vortex surfaces as the time coordinate is shortened. To elucidate the emergence of confinement in a percolating vortex ensemble, consider the following heuristic picture, cf. Fig. 2. Given N random vortex piercings of a plane of area L^2 , the probability that n of the piercings occur within an area A spanned by a Wilson loop is binomial. Considering for definiteness the $SU(2)$ case, each piercing multiplicatively contributes a center element factor -1 to the Wilson loop, i.e., for n piercings within the loop, it takes the value $(-1)^n$. Summing over all possibilities with the

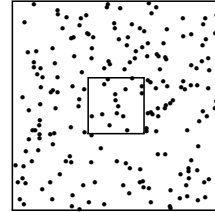


Figure 2. Confinement induced by random linkings of vortices with Wilson loops. A two-dimensional plane of area L^2 containing a Wilson loop spanning an area A is pierced by vortices at random locations.

proper binomial weight yields

$$\begin{aligned} \langle W \rangle &= \sum_{n=0}^N (-1)^n \binom{N}{n} \left(\frac{A}{L^2} \right)^n \left(1 - \frac{A}{L^2} \right)^{N-n} \\ &= \left(1 - \frac{A}{L^2} \right)^N \exp(2A) \end{aligned}$$

where L^2 has been eliminated in favor of the planar density $\rho = N/L^2$, and in the final step, the limit of a large universe $N \rightarrow \infty$ at constant ρ is taken. Thus, one obtains an area law for the Wilson loop, with the string tension determined by the vortex density. The crucial assumption in this argument is the independence of the piercing points. This can only be accurate if the vortices percolate as in the left panel of Fig. 1. In the absence of percolation, there is an upper bound on the size of a vortex cluster. As a consequence, piercing points come in pairs less than this maximal size apart; if a vortex pierces a plane in one direction, it must return to pierce it again in the other direction, because it must ultimately close. Evaluating the Wilson loop in complete analogy to above, only with piercing point pairs distributed on the plane, gives a perimeter law. Note furthermore that adjoint Wilson loops yield zero string tension, since they have unit value even when encircling a single center vortex; the center vortex picture yields the correct n -ality dependence of string tensions by construction.

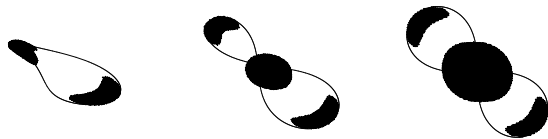


Figure 3. Topological charge density on a writhing, self-intersecting vortex surface. The thin line is to guide the eye as to the location of the geometrical center of the (thick) vortex; this is a vortex loop (left) which is twisted until it becomes a figure eight and self-intersects (right). The scatter plot indicates locations where the topological charge density exceeds a certain threshold. In the center and right-hand figures, the signature of the self-intersection is evident; on the other hand, the kidney-shaped contributions at the periphery originate from vortex writhe [26].

3.1.2. Topology

Topological charge density is generated by vortex self-intersections and vortex writhe. In the $SU(2)$ case, self-intersections carry topological charge ± 2 , whereas topological charge density due to writhe in general is distributed continuously along vortex surfaces. An instructive example illustrating both types of contribution was presented by F. Bruckmann and the author in [26], cf. Fig. 3. In the case of surfaces made up of elementary squares on a hypercubic lattice, contributions of writhe become discrete, concentrated on lattice sites, with modulus less than $1/2$ at each site. In realistic vortex ensembles, cf. section 3.1.3, the contributions of vortex writhe to the topological charge are statistically far more important than the ones due to vortex self-intersections.

Globally, generic vortex world-surfaces are nonorientable. If one attempts to rotate the associated field strength into an Abelian gauge, then, as one orients the field, say, into the positive 3-direction in color space along the vortex, one encounters frustrations where one is forced to switch to the negative 3-direction. At the frustrations, magnetic flux corresponding to an Abelian monopole is supplied to or taken from the vortex, cf. Fig. 4. Center vortex surfaces in Abelian gauges thus naturally contain Abelian magnetic

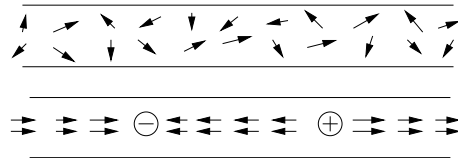


Figure 4. Magnetic monopoles distributed along vortices in Abelian gauges due to vortex nonorientability (from [27]).

monopoles. In fact, they are necessary to generate a global topological charge; on oriented vortex surfaces, the local contributions to the topological charge globally add up to zero [28].

The real physical difference to the dual superconductor picture, cf. section 3.2, thus does not lie in the presence or absence of monopoles, but in the form taken by the field strength emanating from those monopoles. In the dual superconductor picture, a monopole is assumed to generate a radial magnetic Coulomb field, whereas in the vortex picture, the field strength is constricted into center vortex fluxes. Of course, in the latter picture, the vortices are taken to be the primary degrees of freedom, and the behavior of the monopoles on the vortices is seen as a consequence of the primary vortex dynamics. In the dual superconductor, the monopoles are assumed to be the primary degrees of freedom.

3.1.3. Dynamics of the random vortex world-surface model

As discussed further above, it is important to test whether a particular set of infrared collective gluonic degrees of freedom can indeed generate the main features of the strong interaction vacuum on the basis of a weakly coupled dynamics. To this end, a random vortex world-surface model has been introduced and studied [29,30,31,32,33]. In this model, the vortex surfaces are composed of elementary squares on a hypercubic lattice. The spacing of this lattice is a fixed physical quantity interpreted as mimicking the effects of the finite vortex thickness; parallel thick vortices cannot be distinguished anymore if they approach each other more closely than their radius, which turns out to be roughly 0.4 fm (the scale is ul-

timately set by the zero-temperature string tension). The lattice spacing at the same time provides the fixed ultraviolet cutoff characteristic of any infrared effective model. The random vortex surface ensemble is generated by Monte Carlo methods, weighted by an action which controls vortex curvature at short distances. On long distance scales, the vortex surfaces are thus random and uncorrelated.

On the basis of these assumptions, the random vortex world-surface model reproduces both the confined and the deconfined phases of Yang-Mills theory, for SU (2) color [29] as well as SU (3) color [32], in accordance with the heuristics presented further above. The only dimensionless parameter of the model, namely the coupling strength in the curvature action, is fixed by fitting the ratio of the deconfinement temperature to the (square root of the) zero-temperature string tension obtained in the corresponding Yang-Mills theory. The model correctly predicts a second order deconfinement phase transition for SU (2) color and a very weakly first order transition for SU (3) color. Also the behavior of the spatial string tension in the deconfined phase is described correctly. For SU (3) color, baryonic static quark configurations obey a Y area law [33]. Beyond the confinement properties, also the SU (2) topological susceptibility predicted by the model agrees quantitatively with the one obtained in Yang-Mills theory [30], and chiral symmetry is broken spontaneously in the confined phase, with a natural value for the (quenched) chiral condensate [31].

3.1.4. Vortex detection in lattice gauge configurations

To study vortex physics in full lattice gauge theory, it is necessary to devise methods to detect and isolate vortices in lattice gauge configurations. Two main approaches have been studied in this respect. One approach relies on gauges of the maximal center type [34], such as defined by the gauge condition (in the case of SU (2) color) $\max_i \int \text{tr} U_i^2$, where the U_i are the link variables and the maximization is carried out over all gauge transformations thereof. The gauge is thus chosen such as to concentrate the link variables near the center elements of the gauge group. In

a second step, center projection, $U \rightarrow \text{sign tr} U$, residual deviations away from those center elements are discarded, yielding a Z (2) gauge configuration, which is associated with vortex world-surfaces on the dual lattice in canonical fashion (negative plaquettes in the Z (2) configuration are pierced by vortices). Using this two step-procedure, one aims to concentrate as much of the relevant physical information on the collective center vortex degrees of freedom as possible.

After the introduction of maximal center gauges, it was noted that string tensions measured in the projected vortex ensemble depend substantially on the selection of Gribov copies when fixing the gauge [35]. The precise gauge fixing and projection procedure needs to be selected carefully in order to ensure that the resulting projection vortex ensemble captures the main infrared physics. While the situation in the case of SU (3) color is still unclear [36], for SU (2) color, a quite successful procedure can be constructed, which in fact turns out to be a hybrid [37] of maximal center gauge fixing and the second major method of detecting vortices, namely the Laplacian center gauge.

The Laplacian center gauge [38] is free of Gribov copy selection issues. It is defined via eigenvectors of the lattice adjoint Laplacian operator. Two such eigenvectors are chosen, usually the ones with the lowest eigenvalues; vortices are located on the two-dimensional submanifolds of space-time where the eigenvectors become collinear in color space. In addition, Abelian monopoles are located on the lines where the eigenvector corresponding to the lowest eigenvalue vanishes. Thus, by construction, the monopoles are located on the vortex surfaces in this approach.

Ultimately, it would be desirable to devise a gauge-invariant vortex detection method. In principle, the desired information is contained in the Wilson loops evaluated in a given gauge configuration; in practice, extracting vortices from them is a difficult pattern recognition problem, especially since the density of thick vortices in the Yang-Mills vacuum is such that the vortices overlap considerably; for a recent investigation which touches upon this issue, cf. [39].

3.1.5. Results of lattice studies

Based on the vortex detection procedures described above, a number of vortex properties have been investigated. They include (the following are results for SU (2) color, except where otherwise indicated):

Center dominance of the string tension: Extracting the vortex content of lattice configurations and measuring Wilson loops in the resulting vortex ensemble, one recovers the full Yang-Mills string tension [37,40]. As mentioned above, when using the maximal center gauge, one must be judicious in dealing with the Gribov problem.

Vortex-limited Wilson loops: Having identified the vortex content of the Yang-Mills ensemble, one can select subensembles in which a large region of a given lattice plane is not pierced by a center projection vortex or in which this region is pierced by exactly one vortex. Evaluating a Wilson loop in the aforementioned region using the full Yang-Mills configurations contained in either subensemble, and taking the ratio of the values obtained, one ends up with a ratio approaching 1 as the Wilson loop becomes large [37]. This indicates that the thin center projection vortex indeed represents the location of a thick center flux in the full Yang-Mills configuration; when the Wilson loop becomes sufficiently large, it encompasses the full flux, yielding the appropriate center phase. Effects of other fluctuations around this center flux are largely canceled in the ratio.

Vortex removal also removes all non-perturbative effects: Center projection yields a Z (2) lattice configuration with non-trivial center phases on selected links. Removing those center phases from the links of the full Yang-Mills configuration defines the vortex-removed configuration. In the vortex-removed ensemble, the string tension and the chiral condensate vanish, and all configurations are in the topological charge zero sector [41].

Deconfinement transition as a percolation transition: At finite temperatures, the center projected vortex ensemble reproduces the deconfinement phase transition, at which it displays a percolation transition in accordance with the heuristics given further above [42,43].

Roughening: The center projection vortex density is suppressed within the chromoelectric flux tube between static sources, and can be used as a measure of the width of that flux tube. Varying the distance between the static sources, evidence of roughening is obtained [44,45].

Maximal Abelian gauge monopoles on vortices: While in the Laplacian center gauge, monopoles are located on vortices by construction, one also finds empirically that maximal Abelian gauge monopoles are located on maximal center gauge vortices [27, 46]. Moreover, the action in the monopole region is not distributed isotropically, but is collimated in the directions of the vortex.

Topological susceptibility: The center-projected vortex ensemble generates a topological susceptibility compatible with the one obtained in full Yang-Mills theory [47].

Vortices and Higgs fields: Extracting center projection vortices from an SU (2)-Higgs ensemble, no vortex percolation is observed in the Higgs (screening) phase [48].

SU (3): Generalizing to SU (3) color, center dominance of the string tension is again observed for the center vortices extracted via the Laplacian center gauge [40]; significant deviations from center dominance have been reported when gauges of the maximal center type are used [36], presumably due to the Gribov problems already observed in the SU (2) case.

3.2. The dual superconductor

Abelian magnetic monopoles are quantized sources and sinks of Abelian magnetic flux. To be definite, one can select a $U (1)^{N-1}$ subgroup

of $SU(N)$ Yang-Mills theory by fixing the color direction of covariantly transforming quantity of one's choosing; monopoles are sources and sinks of flux with respect to that $U(1)^{N-1}$. The ensemble of monopole world-lines in space-time can be cast in terms of a field theory.

3.2.1. Confinement

Motivated by the Ginzburg-Landau description of type-II superconductors, in which magnetic flux is constricted into flux tubes, in the dual superconductor picture one formulates a dual relativistic analogue, in which chromoelectric flux is constricted, thus generating confinement. The role of the (electrically charged) Cooper pairs is taken over by Abelian magnetic monopoles. The corresponding Ginzburg-Landau Lagrangian is the one of the dual Abelian Higgs model,

$$L = \frac{1}{4} G^2 + j(\partial_\mu + igC)_\nu^2 + \frac{1}{4} (\partial_\mu v)^2$$

Here, ∂_μ describes the monopole field, and C is a dual $U(1)^{N-1}$ gauge field inducing a dual field strength G . This theory contains Nielsen-Olesen vortex solutions of chromoelectric flux if the monopoles are condensed, i.e., if the monopole world-lines percolate; thus, a confining potential between static quarks is induced. When monopoles are not condensed, chromoelectric sources are deconfined; both the confined and the deconfined phases can therefore be described in a model based on Abelian magnetic monopoles.

However, due to the Abelian character of the description, adjoint $SU(N)$ sources, which are doubly charged with respect to the $U(1)^{N-1}$ gauge group of the effective model, are also confined. One does not obtain the correct n -ality dependence of string tensions in the dual superconductor picture. As will be discussed in greater detail below, the crucial truncation leading to this behavior lies in neglecting the off-diagonal gluon degrees of freedom present in the underlying Yang-Mills theory. This is often justified with the argument that these fields acquire a mass and should therefore decouple. This appears to be fallacious, and to restore the effect of the off-diagonal gluons in the dual superconductor, one needs to add a coupling to charge-2 matter fields. These, indeed, screen adjoint $SU(N)$

sources, restoring the correct n -ality dependence of string tensions.

3.2.2. Topological charge

Topological charge implies the presence of magnetic monopoles, as is apparent from the following observations:

Only non-oriented vortices (i.e., ones containing monopoles) carry global topological charge.

Instantons in Abelian gauges exhibit monopoles (and vortices).

Calorons generically consist of monopole constituents.

However, conversely, monopole positions in general are not enough to specify topological charge; one needs to specify the magnetic field strength emanating from the monopoles (except in special gauges, such as the Polyakov gauge). One particular such specification indeed generates the correct topological susceptibility, namely collimating the magnetic flux into vortices, as embodied in the random vortex world-surface model [30]. However, as far as the author is aware, there is no analogous calculation of the topological susceptibility in a monopole Coulomb gas model describing the standard dual superconductor scenario. Similarly, there appears to be no evaluation of the chiral condensate in such a model.

3.2.3. Monopole detection in lattice configurations

In principle, monopoles can be defined by finding the eigenvalues in color space of a covariantly transforming quantity of one's choosing (monopoles being located where two eigenvalues are degenerate); in practice, the maximal Abelian gauge [49], defined by the gauge condition $\max_P \text{tr}_i U_i^3 U_i^Y$, which renders the gauge fields as diagonal as possible, is used to determine the monopole content of a $(SU(2))$ lattice gauge configuration. This gauge leaves a residual $U(1)$ gauge symmetry under which the diagonal part of the gauge field transforms as a photon, whereas the off-diagonal fields transform as charge-2 matter fields. In a second step,

Abelian projection, residual off-diagonal parts in the gauge field are discarded and the diagonal fields are rescaled such as to preserve unitarity of the link variables. Monopole positions can be identified by searching for Dirac string fluxes leaving elementary lattice cubes. Beyond Abelian projection, one can furthermore define monopole projection, in which only the information on the monopole positions is kept and new configurations are constructed in which magnetic Coulomb fields are associated with the monopoles [50,51]. This corresponds most closely to the dual superconductor picture. It should be emphasized that, in contrast to monopole projection, Abelian projection introduces no a priori constraint on the form of the Abelian fields; the form of these fields is still determined by the dynamics and they could, e.g., be vortices. Indeed, being generated using the full Yang-Mills dynamics, the gauge fields in the Abelian projected configurations contain the effects of the off-diagonal gluon dynamics. By contrast, in monopole projection, merely the monopole positions still contain the effects of the full dynamics, whereas the field strength emanating from the monopoles is Coulombic by construction.

Before continuing with the discussion of lattice results obtained in practice using these projected configurations, it should be noted that also further conceptual refinements have been proposed recently regarding the consistent definition of electric and magnetic currents in the Abelian projection framework [52].

3.2.4. Results of lattice studies

A variety of issues have been investigated based on the Abelian and monopole projection techniques discussed above. They include:

Abelian dominance: Evaluating Wilson loops using Abelian projected configurations yields (92–4)% of the full fundamental string tension [53,54]. Adjacent sources are not connected.

Monopole dominance: Using monopole projected configurations to compute Wilson loops, one recovers 87% of the full fundamental string tension [50,51]. However, ad-

joint sources are connected [27].

Percolation properties: While the world-lines of maximal Abelian gauge monopoles percolate in the connected phase, they cease to percolate in the deconfined phase, both in the quenched case and in the case of two dynamical quark flavors [55].

Flux tube properties: Examining the structure of the monopole and photon fields in the region of the chromoelectric flux tube between static color sources, the parameters of the corresponding Nielsen-Olesen vortex solution of the dual Abelian Higgs model can be identified. This has been investigated both for the quenched case [56,57,58,59] and for the case of two dynamical quark flavors [59]. No roughening is reported.

Baryonic configurations: The potential of baryonic static quark configurations evaluated using the Abelian projected ensemble obeys a Y law [55].

Fundamental string breaking: Fundamental string breaking at large distances between static quark sources in the presence of two flavors of dynamical quarks has been observed using Abelian projected configurations [60].

Monopole action and entropy: The effective action, world-line length distribution and entropy have been extracted for maximal Abelian gauge monopoles [61].

Magnetic disorder parameter: A magnetic disorder parameter has been defined in order to study magnetic monopole condensation, in particular its relation to the deconfining phase transition [62,63,64,65,66,67].

Adjacent string breaking: The dual superconductor incorrectly connects adjacent color sources. This can be remedied by coupling the dual Abelian Higgs model to charge-2 matter fields, which screen adjacent

sources [68]. Such a coupling is indeed natural, since the underlying Yang-Mills theory contains off-diagonal gluon fields, which transform as charge-2 matter fields in the maximal Abelian gauge. The importance of this coupling has also been corroborated by the observation that the charge-2 matter fields provide an essential part of the total action in Abelian projected lattice Yang-Mills theory [69]. However, pursuing this train of thought further, the dynamics of the charge-2 matter fields have the additional effect that monopoles are arranged into chain-like structures [70], which can be identified as vortices [1]. Thus, restoring the correct n -ality dependence of string tensions in the dual superconductor model by introducing charge-2 matter fields ultimately guides one towards adopting the vortex picture.

Monopole world-line correlations: The world-lines of maximal Abelian gauge monopoles are not random walks on infrared scales, but exhibit long-range correlations characteristic of the monopoles being associated with two-dimensional surfaces in space-time [71]. This observation is consistent with the fact that maximal Abelian gauge monopoles are located on center vortex world-surfaces, the dynamics of which determine monopole behavior.

3.3. Topological charge lumps

3.3.1. Merons

A (SU(2) color) meron located at the space-time origin can be described by the gauge field

$$a_\mu(\mathbf{x}) = \frac{a}{x^2 + \frac{1}{2}} \frac{x_\mu}{2}$$

with the 't Hooft symbol \tilde{a} . For width parameter $\beta = 0$, this is a (albeit singular) solution of the classical Yang-Mills equations of motion. Merons carry topological charge $1=2$; since their field strength behaves as $1=x^2$ at large distances x , the action of a single meron is logarithmically divergent. However, one can construct a meron gas with finite action density if the meron color

orientations are suitably correlated [72]. Using the ansatz

$$A_\mu(\mathbf{x}) = \sum_{i=1}^M h_i a_\mu(\mathbf{x} - \mathbf{z}_i) h_i^{-1}$$

for a configuration of M merons at positions \mathbf{z}_i , where the h_i are color rotation matrices, one can define a meron ensemble by summing over all \mathbf{z}_i and h_i weighted with the Yang-Mills action. In practice, the ensemble is treated using Monte Carlo methods; note that the update is non-local, since any given meron interacts with all other merons. This model induces nontrivial color correlations between the merons, which result in a confining linear potential between static quarks. Using the string tension to fix the scale, one simultaneously obtains a topological susceptibility which agrees quantitatively with the one obtained in SU(2) Yang-Mills theory. It would be interesting to further investigate the correlations between the merons, in particular with a view to understanding whether higher-dimensional collective excitations are induced by the dynamics of the model.

3.3.2. Instantons

Instantons are regular solutions of the classical Yang-Mills equations of motion which are localized in space-time and carry topological charge ± 1 . They are the basis for the highly successful instanton liquid model of the strong interaction vacuum, which describes the $U_A(1)$ anomaly, the spontaneous breaking of chiral symmetry, and a wealth of hadron phenomenology associated with these effects, cf. the review [73]. However, there is no confinement in the instanton liquid model.

A detailed discussion of methods used for detecting instantons in lattice gauge configurations constitutes a separate topic which lies beyond the scope of this review. Tests of the instanton picture within the framework of lattice gauge theory have revealed the following results [74]:

The procedure of cooling lattice configurations can be used as a filter to retain only classical solutions, i.e., instantons. Using cooled configurations to evaluate light hadron correlators, one obtains essentially

the same light hadron phenomenology as when using the full lattice configurations. On the other hand, confinement disappears.

There are correlations between the positions of low virtuality quark modes in the full configurations and the positions of instantons in the cooled configurations.

Low virtuality quark modes dominate light hadron physics. Truncating the spectrum of the Dirac operator in the lattice gauge ensemble to include only these modes yields a good approximation to hadronic correlators.

These findings suggest viewing the low virtuality quark modes dominating light hadron phenomenology as being generated by instantons in the strong interaction vacuum. Indeed, an isolated instanton gives rise to a zero mode of the Dirac operator, and an ensemble of not completely isolated instantons therefore generates a band of near-zero modes (thus inducing the spontaneous breaking of chiral symmetry via the Caser-Banks relation). On the other hand, it is just as consistent with the above observations that a different class of topological charge lumps induces the low virtuality quark modes, and that replacing these by modes generated by instantons represents only a mild (and very useful) idealization. Note that, even if such a different class of topological charge lumps is present in the full lattice configurations, it will be reduced to instantons under cooling, since the latter are minima of the Yang-Mills action. The fact that the instantons in the cooled lattice configurations faithfully reproduce only partial aspects of the strong interaction vacuum, namely the correct ensemble of low virtuality quark modes, but not confinement, points toward the relevant degrees of freedom carrying topological charge in that vacuum being different from instantons.

Motivated by the strongly correlated confinement model described in the previous section, a completely analogous strongly correlated instanton model has been investigated very recently [75]. This model indeed also produces confinement of fundamental color sources, and,

moreover, does not confine adjoint color sources [76]. Again, it would be interesting to further investigate the correlations between the instantons, especially whether higher-dimensional collective excitations are induced by the dynamics of the model. Also modifications of instanton liquid phenomenology by the color correlations present in this model need to be investigated.

3.3.3. Calorons

Calorons are solutions of the classical Yang-Mills equations of motion on space-times with compact directions, such as the ones used to describe finite temperatures; they carry quanta of topological charge. Calorons display striking space-time properties, generically consisting of monopole constituents, where it should be emphasized that these monopoles are defined in a fully gauge-invariant fashion [77,78]. No gauge fixing procedure is necessary to identify the constituents in the caloron solutions. It seems tempting to speculate that confinement may be understood in the caloron picture on the basis of these monopoles.

Calorons and their monopole substructure have recently been detected in lattice gauge configurations via cooling methods [79] as well as via associated quark zero modes [80,81,82]. The observations in these studies suggest that the topological charge distribution in the QCD vacuum is more fragmented and structured than in an ensemble of uncorrelated instanton-like lumps. This is corroborated by investigations which indicate the presence of a long-range low-dimensional topological charge structure in the QCD vacuum [83].

4. SYNOPSIS

Of the collective infrared gluonic degrees of freedom considered, center vortices are the only ones for which a weakly coupled model has been formulated which reproduces the main non-perturbative features of the strong interaction vacuum. This supports the notion that center vortices are the actual relevant degrees of freedom in the infrared sector. Going from the vortex picture to the dual superconductor picture and to weakly coupled models based on topologi-

cal charge lumps, an increasing level of truncation of the degrees of freedom and the associated nonperturbative physics is introduced. Conversely, if one wishes to nevertheless describe the full spectrum of nonperturbative effects using Abelian monopoles or topological charge lumps, one is forced to formulate models with progressively stronger correlations to recover all the relevant physics. This is a signature that those degrees of freedom are really combined into other collective degrees of freedom which more accurately characterize the strong interaction vacuum. Nevertheless, if one wishes to focus on a particular type of nonperturbative effect, the more strongly truncated models can be very useful; this is best evidenced by the wealth of phenomenological results obtained in the instanton liquid model, unparalleled by any of the other approaches, despite the absence of confinement in this model.

In detail, recent work has led to a convergence of the vortex and the dual superconductor pictures. Both pictures contain Abelian monopoles; however, in the vortex picture, they are a secondary consequence of the nonorientability of vortex world-surfaces and their behavior is determined by the primary vortex dynamics. As a case in point, monopoles inherit the percolation properties of the vortex surfaces on which they are located; the deconfinement transition can be equally detected as a percolation transition in the monopole world-lines or the vortex world-surfaces. Going from the vortex picture to the dual superconductor picture, one introduces two truncations. On the one hand, the field strength sourced at the monopoles is assumed to take a radial Coulomb form instead of being constricted into vortex fluxes; on the other hand, monopole world-lines are assumed to behave as random walks in space-time instead of displaying correlations characteristic for them being located on two-dimensional random surfaces. The former truncation in particular leads to the loss of the correct n -ality dependence of string tensions; not only fundamental color sources, but also adjoint ones are confined in the dual superconductor. Moreover, lattice studies have indeed shown that monopole world-lines do not behave as random walks, but do display correlations charac-

teristic of them being located on vortex surfaces [71]. To remedy these truncations, one either has to revert to the vortex picture or, which is presumably equivalent, resort to more complicated models of Abelian monopoles coupled to charge-2 matter fields (which are descendants of the off-diagonal gluons in Yang-Mills theory). This coupling, which is discarded in the standard dual superconductor scenario, is evidently instrumental in constricting chromomagnetic flux into vortices, thus inducing the correct n -ality dependence of string tensions [70,1].

The connection between the vortex picture and models based on topological charge lumps is not yet understood in quite as much detail. Center vortices contain topological charge lumps induced by vortex writhe and vortex self-intersections, cf. Fig. 3. It seems plausible that the physics controlled by this topological density can be well described by models based directly on topological charge lumps; indeed, the instanton liquid model is very successful in describing the effects of spontaneous chiral symmetry breaking and the axial $U_A(1)$ anomaly. Nevertheless, by formulating weakly coupled models of this type, which, e.g., do not include any correlations characteristic of the topological charge being located on, and induced by, vortices, one is evidently truncating relevant physics; confinement is lost. Accordingly, evidence from lattice studies is mounting that the topological charge distribution in the QCD vacuum is indeed more fragmented and structured than suggested by a picture of uncorrelated instanton-like lumps [82,83]; topological charge must be organized into higher-dimensional long-range collective degrees of freedom to recover the full physics. This is also indicated by the recent construction of strongly correlated meron and instanton models which do display confinement [72,75]. However, the precise nature of these correlations and the collective degrees of freedom induced by them remains to be studied in more detail; the aforementioned new meron and instanton models may turn out to be very valuable laboratories in this respect. They indicate that, in particular, the color orientations of topological charge lumps must be properly aligned.

Finally, the intriguing cross-connection be-

tween calorons and monopoles should be noted; calorons are not unstructured lumps of topological charge, but generically consist of monopole constituents, where it should be emphasized that these monopoles are defined in a gauge-invariant manner, as opposed to the maximal Abelian gauge monopoles the dual superconductor scenario usually refers to. Nevertheless, this connection suggests that confinement in the caloron picture may possibly be generated through these monopole constituents. It would also be interesting to understand in detail whether, and how, vortex flux may enter the caloron picture.

Acknowledgments

The author is grateful to the Local Organizing Committee and the International Advisory Committee for the opportunity to present this review, and to the many colleagues who have furnished their insights on diverse topics touched upon here, in particular J. Negele and P. van Baal. This work was supported by the U.S. DOE under grant number DE-FG 03-95ER 40965.

REFERENCES

1. J. Greensite, *Prog. Part. Nucl. Phys.* 51 (2003) 1.
2. J. Greensite, S. Olejnik and D. Zwanziger, *Phys. Rev. D* 69 (2004) 074506.
3. K. Langfeld and L. Moyaerts, [hep-lat/0406024](#).
4. S. Furui and H. Nakajima, [hep-lat/0403021](#).
5. P. O. Bowman, U. M. Heller, D. B. Leinweber, M. B. Parappilly and A. G. Williams, *Phys. Rev. D* 70 (2004) 034509.
6. A. Cucchieri, T. Mendes and A. R. Taurines, [hep-lat/0406020](#).
7. J. Gattnar, K. Langfeld and H. Reinhardt, *Phys. Rev. Lett.* 93 (2004) 061601.
8. K. Holland, P. Minkowski, M. Pepe and U.-J. Wiese, *Nucl. Phys. B* 668 (2003) 207.
9. K. Holland, M. Pepe and U.-J. Wiese, [hep-lat/0312022](#).
10. P. de Forcrand and O. Jahn, *Nucl. Phys. B* 651 (2003) 125.
11. A. Barresi, G. Burgio, M. D'Elia and M. Muller-Preussker, [hep-lat/0405004](#).
12. L. Del Debbio, H. Panagopoulos and E. Vicari, *JHEP* 0309 (2003) 034.
13. B. Lucini, M. Teper and U. Wenger, *JHEP* 0406 (2004) 012.
14. E. T. Tomboulis, [hep-lat/0311022](#).
15. S. Kratochvila and P. de Forcrand, *Nucl. Phys. B* 671 (2003) 103.
16. M. Luscher and P. Weisz, *JHEP* 0109 (2001) 010.
17. V. G. Bomyakov, M. N. Chernodub, H. Ichie, Y. Komatsu, Y. Mori, Y. Nakamura, M. I. Polikarpov, G. Schierholz, A. A. Slavnov, H. Stuben, T. Suzuki, P. V. Uvarov and A. I. Veselov, [hep-lat/0401014](#).
18. M. Luscher and P. Weisz, *JHEP* 0207 (2002) 049.
19. K. J. Juge, J. Kuti, F. Maresca, C. Morningstar and M. Peardon, *Nucl. Phys. Proc. Suppl.* 129 (2004) 703.
20. K. J. Juge, J. Kuti and C. Morningstar, [hep-lat/0401032](#).
21. M. Caselle, M. Hasenbusch and M. Panero, *JHEP* 0405 (2004) 032.
22. M. Caselle, M. Pepe and A. Rago, [hep-lat/0406008](#).
23. P. Majumdar, *Nucl. Phys. B* 664 (2003) 213.
24. Y. Komatsu, M. Komatsu and P. Majumdar, *Nucl. Phys. B* 692 (2004) 209.
25. O. Jahn and P. de Forcrand, *Nucl. Phys. Proc. Suppl.* 129 (2004) 700.
26. F. Bruckmann and M. Engelhardt, *Phys. Rev. D* 68 (2003) 105011.
27. J. Ambjorn, J. Giedt and J. Greensite, *JHEP* 0002 (2000) 033.
28. M. Engelhardt and H. Reinhardt, *Nucl. Phys. B* 567 (2000) 249.
29. M. Engelhardt and H. Reinhardt, *Nucl. Phys. B* 585 (2000) 591.
30. M. Engelhardt, *Nucl. Phys. B* 585 (2000) 614.
31. M. Engelhardt, *Nucl. Phys. B* 638 (2002) 81.
32. M. Engelhardt, M. Quandt and H. Reinhardt, *Nucl. Phys. B* 685 (2004) 227.
33. M. Engelhardt, [hep-lat/0406022](#).
34. L. Del Debbio, M. Faber, J. Giedt, J. Greensite and S. Olejnik, *Phys. Rev. D* 58 (1998) 094501.
35. V. Bomyakov, D. Komarov and M. Polikarpov, *Phys. Lett. B* 497 (2001) 151.

36. K. Langfeld, Phys. Rev. D 69 (2004) 014503.
37. M. Faber, J. Greensite and S. Olejnik, JHEP 0111 (2001) 053.
38. C. Alexandrou, P. de Forcrand and M. D'Elia, Nucl. Phys. A 663 (2000) 1031.
39. S. Cheluvarya, hep-lat/0405018.
40. P. de Forcrand and M. Pepe, Nucl. Phys. B 598 (2001) 557.
41. P. de Forcrand and M. D'Elia, Phys. Rev. Lett. 82 (1999) 4582.
42. M. Engelhardt, K. Langfeld, H. Reinhardt and O. Tennert, Phys. Rev. D 61 (2000) 054504.
43. K. Langfeld, Phys. Rev. D 67 (2003) 111501.
44. V. Bomyakov, A. Kovalenko, M. Polikarpov and D. Sigaev, Nucl. Phys. Proc. Suppl. 119 (2003) 739.
45. V. Bomyakov, A. Kovalenko, M. Polikarpov and D. Sigaev, Nucl. Phys. Proc. Suppl. 129 (2004) 757.
46. A. Kovalenko, M. Polikarpov, S. Syritsyn and V. Zakharov, hep-lat/0402017.
47. R. Bertle, M. Engelhardt and M. Faber, Phys. Rev. D 64 (2001) 074504.
48. R. Bertle, M. Faber, J. Greensite and S. Olejnik, Phys. Rev. D 69 (2004) 014007.
49. A. Kronfeld, M. Laurusen, G. Schierholz and U.-J. Wiese, Phys. Lett. B 198 (1987) 516.
50. H. Shiba and T. Suzuki, Phys. Lett. B 333 (1994) 461.
51. J. D. Stack, S. D. Neenan and R. J. Wensley, Phys. Rev. D 50 (1994) 3399.
52. R. W. Haymaker and T. Matsuki, hep-lat/0310025.
53. T. Suzuki and I. Yotsuyanagi, Phys. Rev. D 42 (1990) 4257.
54. G. Bali, V. Bomyakov, M. Muller-Preussker and K. Schilling, Phys. Rev. D 54 (1996) 2863.
55. V. G. Bomyakov, H. Ichie, Y. Mori, D. Pleiter, M. I. Polikarpov, G. Schierholz, T. Streuer, H. Stuben and T. Suzuki, hep-lat/0401026.
56. G. Bali, C. Schlichter and K. Schilling, Prog. Theor. Phys. Suppl. 131 (1998) 645.
57. Y. Komatsu, M. Komatsu, E.-M. Ilgenfritz, T. Suzuki and M. I. Polikarpov, Phys. Rev. D 68 (2003) 094018.
58. Y. Komatsu, M. Komatsu, E.-M. Ilgenfritz and T. Suzuki, Phys. Rev. D 68 (2003) 114504.
59. V. G. Bomyakov, H. Ichie, Y. Komatsu, Y. Mori, Y. Nakamura, D. Pleiter, M. I. Polikarpov, G. Schierholz, T. Streuer, H. Stuben and T. Suzuki, hep-lat/0310011.
60. V. G. Bomyakov, M. N. Chemodub, H. Ichie, Y. Komatsu, Y. Mori, M. I. Polikarpov, G. Schierholz, H. Stuben and T. Suzuki, hep-lat/0401027.
61. M. N. Chemodub, K. Ishiguro, K. Kobayashi and T. Suzuki, Phys. Rev. D 69 (2004) 014509.
62. J. M. Camona, M. D'Elia, L. Del Debbio, A. Di Giacomo, B. Lucini, G. Paoli and C. Pica, Nucl. Phys. Proc. Suppl. 129 (2004) 689.
63. A. Di Giacomo, hep-lat/0310021.
64. M. N. Chemodub, Phys. Rev. D 69 (2004) 094504.
65. V. A. Belavin, M. N. Chemodub and M. I. Polikarpov, hep-lat/0403013.
66. V. A. Belavin, M. N. Chemodub and M. I. Polikarpov, Phys. Lett. B 554 (2003) 146.
67. J. Frohlich and P. A. Marchetti, Phys. Rev. D 64 (2001) 014505.
68. T. Suzuki and M. N. Chemodub, Phys. Lett. B 563 (2003) 183.
69. M. N. Chemodub, K. Hashimoto and T. Suzuki, Phys. Rev. D 70 (2004) 014506.
70. M. N. Chemodub, R. Feldmann, E.-M. Ilgenfritz and A. Schiller, hep-lat/0406015.
71. V. G. Bomyakov, P. Yu. Boyko, M. I. Polikarpov and V. I. Zakharov, Nucl. Phys. B 672 (2003) 222.
72. F. Lenz, J. W. Negele and M. Thies, Phys. Rev. D 69 (2004) 074009.
73. T. Schafer and E. V. Shuryak, Rev. Mod. Phys. 70 (1998) 323.
74. J. W. Negele, Nucl. Phys. Proc. Suppl. 73 (1999) 92.
75. J. W. Negele, presented at this conference.
76. J. W. Negele, private communication; to be published.
77. F. B. Ruckmann, M. Garcia Perez, D. N. Ogardi and P. van Baal, Nucl. Phys. Proc. Suppl. 129 (2004) 727.
78. F. B. Ruckmann, D. N. Ogardi and P. van Baal, hep-th/0404210.

79. E.-M. Ilgenfritz, B. V. Martemyanov, M. Muller-Preussker and A. I. Veselov, Phys. Rev. D 69 (2004) 114505.
80. C. Gatttringer, E.-M. Ilgenfritz, B. V. Martemyanov, M. Muller-Preussker, D. Peschka, R. Pullirsch, S. Schaefer and A. Schafer, Nucl. Phys. Proc. Suppl. 129 (2004) 653.
81. C. Gatttringer and S. Schaefer, Nucl. Phys. B 654 (2003) 30.
82. C. Gatttringer, Phys. Rev. D 67 (2003) 034507.
83. I. Horvath, S. J. Dong, T. Draper, F. X. Lee, K. F. Liu, N. Mathur, H. B. Thacker and J. B. Zhang, Phys. Rev. D 68 (2003) 114505.